Surface & Coatings Technology 496 (2025) 131649

Contents lists available at ScienceDirect

Surface & Coatings Technology

journal homepage: www.elsevier.com/locate/surfcoat

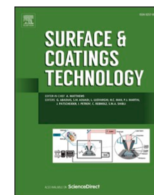

Characterization of protective AlCrON thin films for application on sensor thin films in fused layer modeling processes

Wolfgang Tillmann [a], Julia Urbanczyk [a,*], Maximilian Sonnhof [a], Bernd Künne [b], Michael Mainz [b], Philipp Bengfort [b], Hans-Georg Rademacher [c], Nelson Filipe Lopes Dias [a]

[a] Institute of Materials Engineering, TU Dortmund University, Leonhard-Euler-Straße 2, 44227 Dortmund, Germany
[b] Department of Machine Elements, TU Dortmund University, Leonhard-Euler-Str. 5, 44227 Dortmund, Germany
[c] RIF Institut für Forschung und Transfer e.V., Joseph-von-Fraunhofer-Straße 20, 44227 Dortmund, Germany

ARTICLE INFO

Keywords:
AlCrON
Plastic processing
Tribology
Conductivity
Sensor thin films

ABSTRACT

In plastic processing, the use of sensor thin films is gaining interest for inline measurement to ensure stable process control. However, due to the corrosive and abrasive characteristics of molten plastics, the application of an appropriate protective coating becomes imperative to ensure the functionality of the sensor films. AlCrON thin films demonstrate favorable protective attributes for this purpose. The tribo-mechanical and electrical properties are inherently influenced by the oxygen content. Therefore, a systematic variation of O_2 gas flow rates (10 to 30 sccm in steps of five) during the mid-frequency magnetron sputtering process was employed resulting in the O contents rise from 12.2 at.-% for 10 mln O_2 to 57.6 at.-% for 30 mln O_2. Simultaneously, a change of a polycrystalline structure containing CrN, Cr_2N, and hexagonal AlN to an amorphous structure with increasing O content for AlCrON is observed. This affects the tribo-mechanical properties. The highest polycrystallinity was reached at 25.2 at.-% O resulting in a H/E maximum, with a maximum in hardness of (37.6 ± 2.8) GPa and an elastic modulus of (361.2 ± 20.7) GPa. Here, also the lowest coefficient of friction (CoF) at elevated temperatures was reached with 0.43 against polypropylene (PP) and 0.23 against polyamide (PA). The low CoF correlates with a lower wetting ability of the AlCrON thin film. Regarding the electrical properties AlCrON thin films show insulating characteristics dependent on the O content. The electrical resistance increases with higher O content due to a change into a more ionic structure.

The results show that AlCrON thin films offer promising protective qualities for sensor applications in plastic processing. By adjusting the oxygen content, their tribo-mechanical properties can be optimized for reduced friction and enhanced durability, while their insulating properties are promising for maintaining the functionality of the sensors.

1. Introduction

Material extrusion or fused layer modeling (FLM) is experiencing an increasing demand across industrial, private, and semi-professional applications. Despite being a well-established additive manufacturing technology in rapid prototyping and recognized as one of the most cost-efficient processes it comes with notable shortcomings in the quality and strength of produced components [1,2]. The FLM process in particular is affected by unsteady processing pressures and temperatures within the extruder, which cannot be calculated, measured, or precisely simulated [1,3,4]. As a consequence, the market for products manufactured using FLM processes is limited to those with low demands on strength and tolerance, such as demonstration objects and prototypes, despite the enormous potential of the processes in terms of their economic viability [1,5]. To counteract these difficulties, sensor thin films are gaining increasing interest in research with different approaches to measuring temperature and pressure [6–8]. Additionally, to enhance the mechanical properties of the produced parts themselves fillers can be used [9,10]. Overall, in the processing of synthetic polymers like filaments, the tools and therefore the sensors are exposed to elevated temperatures, high mechanical loads, and corrosive media while withstanding varying levels of tribological stress, depending on the used filler material and amount [9,11]. For this purpose, thin films deposited by physical vapor deposition (PVD) techniques like magnetron sputtering are suitable. The

* Corresponding author.
E-mail address: julia.urbanczyk@tu-dortmund.de (J. Urbanczyk).

https://doi.org/10.1016/j.surfcoat.2024.131649
Received 31 July 2024; Received in revised form 29 October 2024; Accepted 7 December 2024
Available online 9 December 2024
0257-8972/© 2024 The Authors. Published by Elsevier B.V. This is an open access article under the CC BY license (http://creativecommons.org/licenses/by/4.0/).

low thicknesses allow a close-to-couture application even on small and complex geometries [12]. Some promising thin films come into account as protective layers against wear, oxidation, and corrosion for substrates and sensors [13–15]. PVD-deposited CrN thin films show promising properties for plastic processing applications due to enhanced tribo-mechanical properties and higher resistance against corrosion [16,17]. CrN thin films and CrN-Ti multilayered systems were tested under plastic processing conditions. On the one hand, CrN demonstrated a two to three times increase in wear resistance than the CrN-Ti multilayer system, on the other hand, it exhibited a lower performance in chemically aggressive environments compared to multilayered CrN-Ti [16]. To further augment the corrosion resistance of CrN, the system can be expanded by incorporating Al, resulting in CrAlN with increased hardness, enhanced oxidation resistance, and extended resistance against corrosion and wear [18–21]. Higher resistance against oxidation and wear at elevated temperatures and chemical inertness is promoted through the formation of passive oxide layers like Al_2O_3 and Cr_2O_3 [22–24]. Therefore, AlCrON thin films have recently been investigated due to their excellent resistance to oxidation, thermal stability up to 1000 °C, and favorable tribo-mechanical properties, which can be adjusted by the O content [25–28]. Several studies have explored the application of AlCrON thin films in plastic processing. Manz et al. analyzed the adhesion behavior of different synthetic polymers to AlCrON, comparing it with CrN and AlCrN. The study demonstrated that the incorporation of Al and O reduces the adhesion of melted plastic [29]. Contact angle measurements and pin-on-disc tests against polyamide (PA), polycarbonate (PC), and polypropylene (PP) confirmed a decrease in wetting of the molten plastic and coefficient of friction (CoF) with higher O content within the AlCrON thin films [30,31]. Polymethyl methacrylate (PMMA) on the other hand exhibits the highest contact angle at lower O contents, correlating with low friction [32]. Therefore, the chemical composition needs to be adjusted to the specific plastic being processed. The hardness of the thin films is influenced by the Al and O content, with higher O leading to a decrease in hardness and higher Al increasing hardness [28,30]. Since the sensor thin films are powered by current, a certain degree of insulation of the top layer is necessary to prevent short circuits and ensure functionality. As there are hardly any studies on the electrical conductivity of AlCrON thin films, this aspect will also be addressed.

Therefore, AlCrON thin films with different O concentrations by varying the O_2 reactive gas flow rate in a magnetron sputtering process were deposited. The effect on the tribo-mechanical properties against PP and PA as well as its electrical properties regarding using it as a protective layer on sensor thin films for plastic processing applications was investigated.

2. Experimental details

2.1. Deposition setup

The AlCrON thin films were deposited using an industrial magnetron sputtering device CC800/9 Custom (CemeCon AG, Germany). Two Al—24Cr targets (397.5 cm^2 Al with 24 × 1.77 cm^2 Cr plugs along the sputtering track) (CemeCon AG, Germany) and one Cr target (Evochem Advanced Materials GmbH, Germany) were mounted on the magnetron cathodes (see Fig. 1). Hot-working steel (AISI H11) with a Rockwell C hardness 48 HRC and n-type Si(100) wafers served as substrate material and were ultrasonically cleaned for 15 min in ethanol. The deposition chamber was evacuated to a base pressure below 10 mPa. Before deposition, the substrates were etched by Ar^+ ions at a pulsed bias voltage (BV) of $U_b = -650$ V with a mid-frequency of $f = 240$ kHz for 30 min. In the first deposition step, a metallic 200 nm Cr layer was sputtered from the Cr target at a cathode power of $P_c = 4$ kW and a BV of −100 V with a mid-frequency of $f = 250$ kHz in an Ar-regulated pressure of $p = 375$ mPa with an Ar gas flow rate of $q_{Ar} = 300$ sccm. A second 300 nm CrN layer was applied by adding a N_2 gas flow rate of $q_{N2} = 100$ sccm

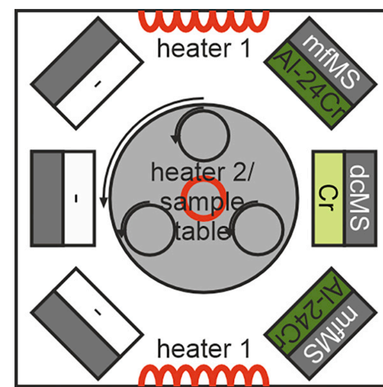

Fig. 1. Magnetron sputtering set up for the deposition of AlCrN and AlCrON thin films deposited at different q_{O2} gas flow rates.

in a N_2-regulated pressure of $p = 375$ mPa and an Ar gas flow rate of $q_{Ar} = 100$ sccm. The AlCrON layer were deposited for $t = 9440$ s by adding O_2 with varying gas flow rates q_{O2} from 10 to 30 sccm in steps of five in an Ar-regulated pressure of $p = 375$ mPa with an Ar gas flow rate of $q_{Ar} = 300$ sccm and a N_2 gas flow rate of $q_{N2} = 100$ sccm. The cathode power of the Al—24Cr targets was set to $P_c = 2$ kW and the pulsed BV was set to $U_b = -100$ V with a mid-frequency of $f = 250$ kHz. The heating power was set to $P_{H1} = 8$ kW and $P_{H2} = 5$ kW, which corresponds to a heater temperature of approximately 720 °C and 750 °C, respectively. For reference, an AlCrN thin film was applied with the deposition parameters mentioned before, but without adding O_2 to the process.

2.2. Characterization of the thin films

The chemical composition was quantitatively determined using an electron probe microanalyzer (EPMA) equipped with four wavelength-dispersive X-ray spectroscopy (WDS). The acceleration voltage was set to 10 keV at a beam current of 20 nA and the beam diameter to 5 μm. The counting times were 10 s for the peak and 5 s for the background signal. To analyze the crystalline phases of the multilayer systems X-ray diffraction (XRD) analysis was performed. Cu-Kα1 radiation with a wavelength of $\lambda = 1.5406$ Å and an x-ray polycapillary lens of 2 mm diameter were used. The locked-couple scan range 2θ was set from 35° to 70° with a scan step of $\Delta 2\theta = 0.034°$ and an exposure time of 1 s. The morphology and topography of the multilayer systems were analyzed by imaging scanning electron microscopy (SEM) in secondary electron mode. The hardness and elastic modulus of the thin films were determined by nanoindentation with a Berkovich diamond tip working in continuous stiffness mode, as proposed by Oliver and Pharr [33]. The hardness and elastic modulus were evaluated up to 10 % of the film thickness to avoid influences of the substrate. A Poisson's ratio of 0.30 for AlCrN [34] and 0.25 for AlCrON [32] was considered for the calculation of the elastic modulus. The adhesion behavior of the AlCrN and AlCrON thin films on the hot-working steel was evaluated in Rockwell C indentation tests at scale A and a load of 588.4 N (60 kgf) according to the German standard DIN 4856:2018–02 [35]. The Rockwell C indents were examined by SEM as well as energy dispersive X-ray spectroscopy (EDS) and categorized into the adhesion strength classes (german *Haftfestigkeit* – HF) from HF1 (excellent adhesion) to HF6 (poor adhesion). From HF1 to HF4 the adhesion strength is rated as permissible and from HF5 to HF6 as impermissible. Additionally, scratch tests were performed using a Revetest (CSM Instruments SA, Switzerland) equipped with a Rockwell C diamond tip with a radius curvature of 200 μm according to DIN EN ISO 20502:2016–11 [36]. The scratches were evaluated in SEM and EDS and the critical loads L_{c2} and L_{c3} were determined. At L_{c2} adhesive failure by chipping of the thin film at the edge of the scratch track appears. Total failure of the thin film by complete exposure of the substrate occurs at L_{c3}. Tribological tests were

carried out using a ball-on-disc high-temperature tribometer (CSM Instruments, Switzerland). Two common plastic materials, polypropylene (PP) and polyamide (PA), were chosen. The tests were carried out in the range of typical tool temperatures during injection molding which are 60 °C (PP) and 85 °C (PA) [37,38]. These temperatures were also used in our previous study [39]. The plastic balls were sliding against the thin films each with a normal load of 5 N, a relative velocity of 10 cm/s, and a sliding distance of 100 m. The tangential force was measured by an inductive sensor, calculating the coefficient of friction (CoF) of the steady-state regime. According to Young, the wettability of the surfaces was determined by the contact angle measurements of water on the AlCrON surface. The contact angle is the angle between the tangent of the water droplet near the coating surface and the coating surface itself [40]. The electrical resistance of the AlCrON thin films was determined using a multimeter (Hameg, Germany). One electrode was contacted on the uncoated substrate underside and the other on the coated substrate top side. The current was measured under an applied test voltage from 2 V to 20 V in steps of 2 in DC mode. The laboratory power supply (Peaktech, Germany) served as the voltage source for testing the dielectric strength of the AlCrON thin films. The samples were secured in an insulated sample holder, with electrical contacts made on both the uncoated and coated sides using cable lugs. The power supply unit allows continuous regulation of the applied voltage within a range of 0 and 32 V. The applied voltage was successively increased from 0 V until a dielectric breakdown occurred, indicated by a measurable current flow between the electrodes, detected by the power supply.

3. Results and discussion

3.1. Chemical composition and structure of the AlCrON thin films

The chemical composition of the AlCrON thin films is listed in Table 1. Additionally, the change in the different elements content is illustrated in Fig. 2. The Al content of the AlCrON thin films shows a decrease with increasing O_2 flow rate q_{O2} (see Fig. 2). For the AlCrN reference sample, the Al content is the highest at (34.65 ± 0.20) at.-% and declines from (32.00 ± 0.32) at.-% at q_{O2} = 10 sccm to (20.66 ± 0.16) at.-% for q_{O2} = 30 sccm. The Cr content remains nearly stable and decreases with a higher O_2 flow rate q_{O2} from (19.34 ± 0.26) at.-% to (17.96 ± 0.20) at.-%. The N content behaves conversely to the increasing O content by reducing from (45.25 ± 0.31) at.-% for AlCrN to (2.66 ± 0.25) at.-% at an O_2 gas flow rate of 30 sccm. Chen et al. explained that AlCrON forms a solid solution where the larger N atoms are replaced by the smaller O atoms leading to metal vacancies as explained by Najafi et al. [28,41]. At a q_{O2} = 15 sccm, the AlCrON thin film exhibits a nearly stochiometric metal-to-non-metal ratio *(Al + Cr)/(O + N)* of 0.96. At this relatively low level of O_2 gas flow rate, the O content increases rapidly until it reaches saturation at q_{O2} = 25 sccm with a ratio *(Al + Cr)/(O + N)* of nearly 2/3 (see Fig. 2). This can be attributed to the higher chemical reactivity, which is given by a higher negative Gibbs energy of Al and Cr toward O compared to N [42]. This indicates a N-doped oxide formation [43]. At this stoichiometric ratio of *(Al + Cr)/(O + N)* about 0.66 AlCrON is referred to as pure oxide [28,43]. With the increase of the O_2 gas flow rate of the AlCrON thin films, the concentration of Ar rises from 0.38 to 1.16 at.-%.

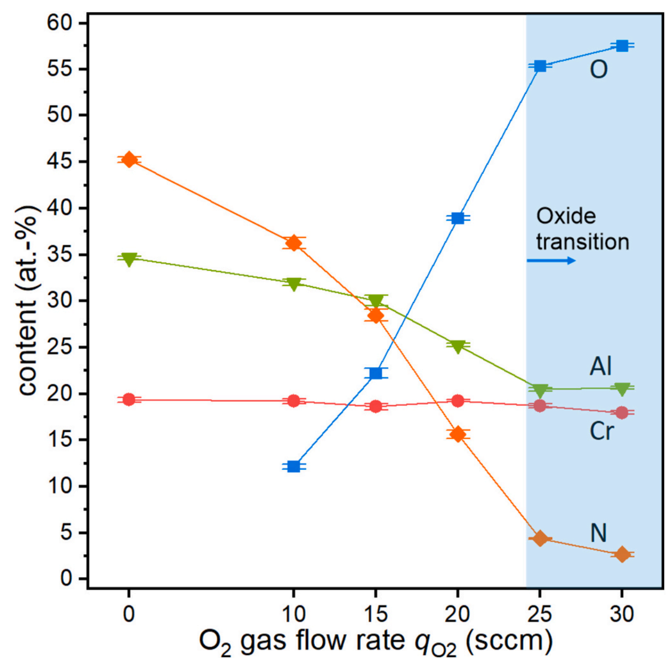

Fig. 2. Chemical composition of the AlCrN and AlCrON thin films deposited at different O_2 gas flow rates, obtained by EMPA.

The change in chemical composition affects the crystalline structure of the AlCrON thin films. Fig. 3 shows XRD patterns of the Cr-CrN-AlCrON multilayered thin films as well as the Cr-CrN-AlCrN reference and the AISI H11 substrate. For all thin films, the diffractions show Bragg reflections of the substrate material, which are assigned to α-Fe at 44.8° and 65.2°. The diffraction from the Cr interlayer at 44.6° and 64.9° overlap with the substrate diffraction.

The AlCrN reference shows a broad diffraction from 37.0° to 38.5°. The broadening comes from the superposition of hexagonal Cr_2N at 37.4°, which could also stem from the CrN layer, and cubic AlCrN at 37.6° from the top layer. The Bragg diffraction around 40.4° and 42.8° can be identified as Cr_2N. Under disregard of the pronounced substrate reflection, the AlCrN thin film shows a preferred orientation along the (111) plane at 37.6°, which can be identified as cubic AlCrN. This is in agreement with the study of Najafi et al. where the AlCrN thin film presents a (111) cubic (Al,Cr)N orientation with additional (200) and (220) diffractions [28].

The addition of 10 sccm O_2 gas flow into the deposition process results in a reflection intensity reduction of the (111) AlCrN diffraction. With rising O content the crystallinity and/or crystal size changes [28]. The diffraction around the 37.5° angle and the broad diffraction around 63.4° can be identified as AlCrN. For 15 sccm O_2 gas flow rate, the intensity at the hexagonal (200) Cr_2N angle increases and an additional broad reflection appears at 43.4° which can be identified as (002) Cr_2N and (200) AlCrN. The investigation of the thermal stability of arc-evaporated AlCrN thin films shows the formation of hexagonal Cr_2N

Table 1
Chemical composition of the AlCrN and AlCrON thin films deposited at different O_2 gas flow rates q_{O2} obtained by EPMA

O_2 flow rate q_{O2} [sccm]		Chemical composition [at.-%]					$\frac{(Al+Cr)}{(O+N)}$	$\frac{O}{(O+N)}$	$\frac{Al}{(Al+Cr)}$
		Al	Cr	N	O	Ar			
AlCrN	–	34.65 ± 0.20	19.34 ± 0.26	45.25 ± 0.31	–	0.75 ± 0.02	1.19	0.00	0.64
AlCrON	10	32.00 ± 0.32	19.21 ± 0.26	36.25 ± 0.62	12.15 ± 0.24	0.38 ± 0.02	1.06	0.25	0.62
	15	30.04 ± 0.55	18.60 ± 0.34	28.46 ± 0.64	22.21 ± 0 54	0.69 ± 0.04	0.96	0.44	0.62
	20	25.26 ± 0.22	19.25 ± 0.11	15.63 ± 0.43	38.93 ± 0.23	0.93 ± 0.04	0.82	0.71	0.57
	25	20.46 ± 0.21	18.73 ± 0.22	4.39 ± 0.06	55.34 ± 0.14	1.06 ± 0.05	0.66	0.93	0.52
	30	20.66 ± 0.16	17.96 ± 0.20	2.66 ± 0.25	57.56 ± 0.18	1.16 ± 0.03	0.64	0.96	0.53

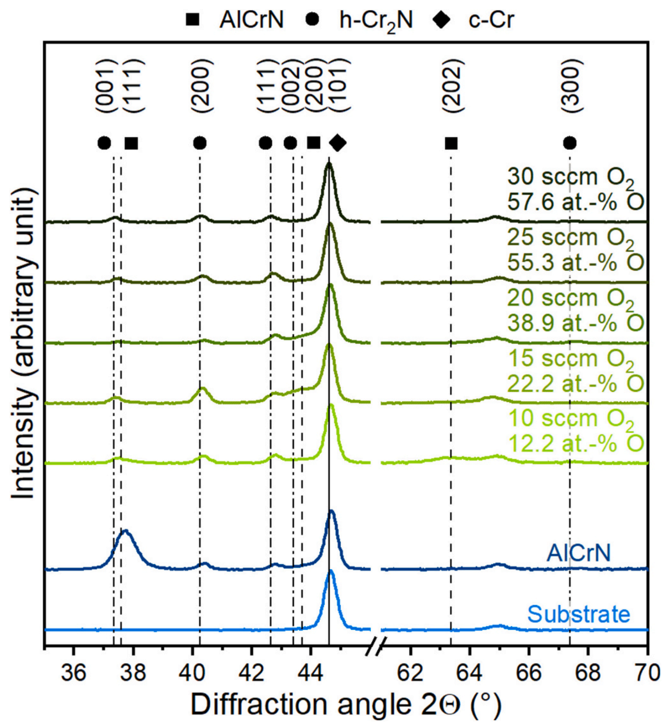

Fig. 3. XRD patterns of the AISI H11 substrate, the AlCrN reference thin film, and the AlCrON thin films deposited at different O_2 gas flow rates q_{O2}.

phases due to the decrease of N [20,44]. This can be transferred to the AlCrON thin film deposited by $q_{O2} = 15$ sccm where O substitutes N atoms in the lattice so that fewer N atoms can react with Cr. What is noticeable is, that AlCrON with an O content of 22.2 at.-% exhibits a more pronounced (002) C_2N reflection and is therefore expected to contain AlCrN and Cr_2N phases. Additionally, a change of the preferential growth changes toward (200) AlCrN. The formation of amorphous phases and changes in surface energy alternate the growth structure from (111) AlCrN for the AlCrN reference thin film to (200) AlCrN for AlCrON [25]. For 20 sccm O_2 gas flow the (200) AlCrN and (200), (002) Cr_2N Bragg reflections are decreasing as O further occupies N atoms positions. Indicating the transformation to an oxide thin film [28]. At 25 sccm and 30 sccm O_2 gas flow rate q_{O2} and regarding the chemical composition, amorphous aluminum oxide phases should be dominant resulting in a diffraction pattern emerging from the substrate and Cr/CrN interlayer system as the AlCrON top layer changes to an x-ray amorphous structure. There are no hexagonal Cr_2O_3 phases detected. At 25 sccm O_2 flow rate, the $O/(O+N)$ ratio reaches 0.93, and at 30 sccm 0.96. Because of the higher Gibbs energy of Al_2O_3 with −1582.3 kJ/mol in comparison to Cr_2O_3 with −1058.1 kJ/mol, it is assumed that mainly amorphous Al_2O_3 with Cr crystallites are formed [45].

Fig. 4 shows the SEM micrographs of the microstructure on the AlCrN reference film and the AlCrON thin film systems. The CrN interlayer grows in a typical columnar structure for all thin films as observed in previous studies [46,47]. With increasing O content, the columnar microstructure of the AlCrN and AlCrON thin film at $q_{O2} = 10$ sccm changes to a compact, amorphous-like morphology at $q_{O2} = 20$ sccm. Najafi et al. observed a similar alternation in the morphology of AlCrON thin films with increasing O contents. Specifying a weakly pronounced columnar microstructure for O content in a range of $0.6 < x \leq 0.97$ [28]. Here the columnar structure is already bearly visible at an O content of 22.2 at.-%. Additionally, the thickness of the AlCrON top layer declines with higher O_2 gas flow rates q_{O2} from (2.05 ± 0.03) μm for AlCrN to (1.06 ± 0.00) μm AlCrOn deposited at $q_{O2} = 30$ sccm (see Fig. 4). This is due to the well-known fact that with the introduction of a higher O_2 gas flow into the deposition process, an increased target poisoning takes through oxidation, thereby reducing the sputtering rate and thus also the deposition rate of AlCrON [31,48]. For AlCrN, the topography exhibits a cauliflower-like structure which changes to a smoother surface with higher O contents due to the change to a glass-like and compact microstructure (see Fig. 4). The surface morphology is similar to the topography of AlCrON thin films in the study of Bagcivan et al. where a reduction in the surface roughness was observed with a higher O_2 gas flow rates [32].

3.2. Mechanical properties of the AlCrON thin films

The change in the O concentration of the AlCrON thin films also affects the mechanical properties hardness H and elastic modulus E. A higher O content leads to a decrease in hardness H and elastic modulus E (see Fig. 5). The AlCrN reference reaches a hardness (H) of (33.9 ± 4.92) GPa and an elastic modulus (E) of (386.5 ± 36.3) GPa. The increase in the O_2 gas flow rate to $q_{O2} = 15$ sccm and thus an O concentration of 22.2 at.-% in the thin films results in a local hardness maximum of (37.7 ± 2.8) GPa, whereas the elastic modulus decreases to (350.6 ± 20.1) GPa. A similar effect was observed in the investigation of Fuentes et al. where the hardness of AlCrON thin films increases, while the elastic modulus decreases up to 30 at.-% O [49]. As the O concentration is

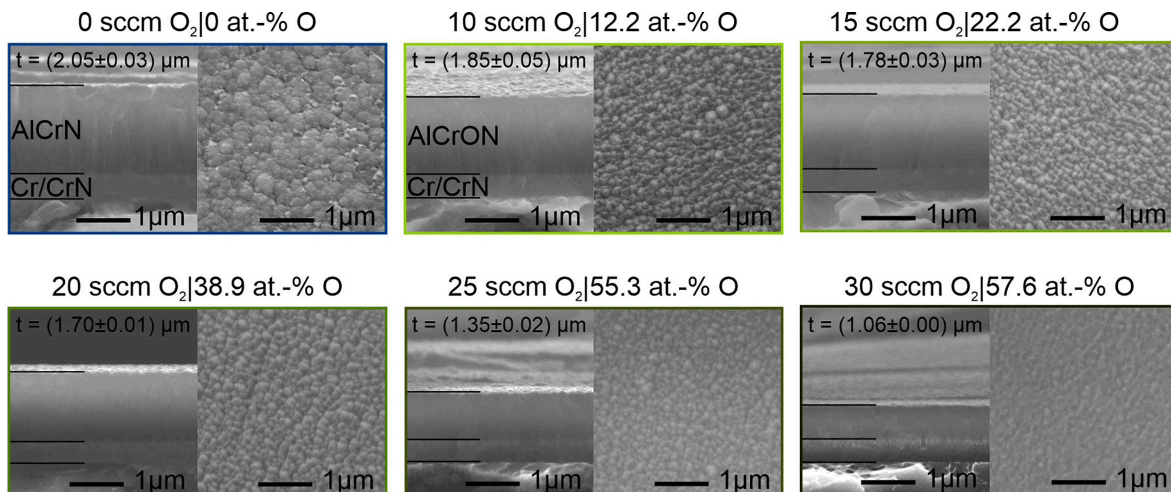

Fig. 4. SEM micrographs of the microstructure including thin film thickness and the surface morphology of the AlCrN and AlCrON thin film system deposited at different O_2 gas flow rates q_{O2}/with different O contents.

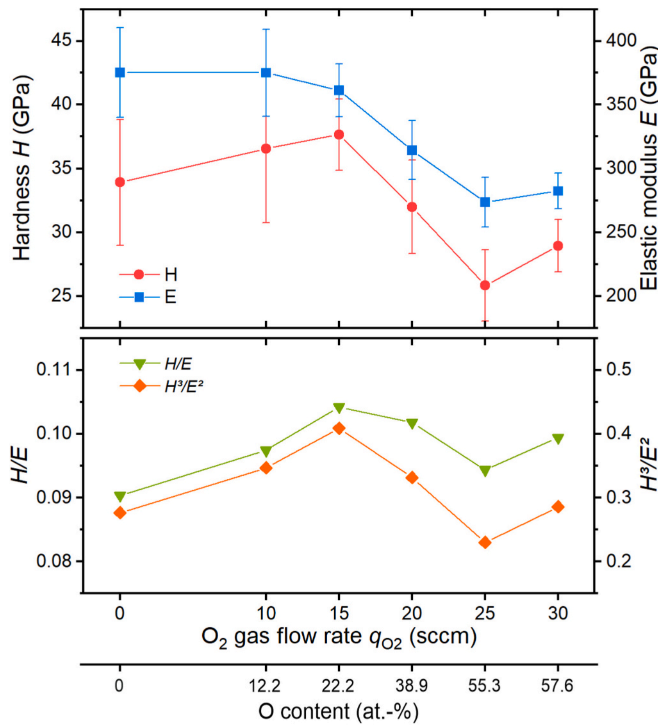

Fig. 5. Hardness H, elastic modulus E, H/E, and H^3/E^2 of the AlCrN and AlCrON thin films deposited at different O_2 gas flow rates q_{O2}/with different O contents.

increased further, the hardness decreases and the elastic modulus reaches its minimum for $q_{O2} = 25$ sccm (O content 55.3 at.-%) with $H = (25.8 \pm 2.8)$ GPa and $E = (273.7 \pm 18.9)$ GPa. For AlCrON with 57.6 at.-% O, an increase in $H = (28.9 \pm 2.1)$ GPa and $E = (282.4 \pm 36.3)$ GPa is observed. The hardness increase from $q_{O2} = 0$ sccm to $q_{O2} = 15$ sccm can be attributed to solid solution strengthening as Al and O dissolve in the CrN lattice, which was observed for low O contents up to 8.8 at.-% [50]. The decrease in hardness after $q_{O2} = 15$ sccm is the result of a change in the growth structure from nitridic to oxynitridic, where the oxynitridic structure exhibits a higher defect density and vacancies in the crystal lattice [28,51]. Additionally, a change from strong covalent to weaker ionic bonding takes place with higher O content which also contributes to a decrease in hardness and elastic modulus [52,53]. When the oxide lattice prevails the hardness and elastic modulus tend to increase again [27,28]. Consequently, the H/E and H^3/E^2 ratios follow a similar trend as the hardness (see Fig. 5). The elastic strain to failure (H/E) and the resistance against plastic deformation (H^3/E^2) [54] reach their local maxima for AlCrON with 22.2 at.-% O. The AlCrON thin film with 22.2 at.-% O exhibits the highest hardness and H/E ratios due to its favorable oxynitridic polycrystalline structure with hard AlCrN and Cr_2N phases (see Fig. 3).

3.3. Adhesion behavior of the AlCrON thin films

The adhesion behavior of the AlCrON thin films was determined with Rockwell C indentation test and scratch test. In Fig. 6 the indents are shown in secondary electron mode (SE) and an enlarged section additionally in backscattered electron mode (BSE). The Rockwell C indents are classified in HF 2 to HF 3 and are therefore admissible [35]. The AlCrN reference shows radial cracks and occasional spalling at the indent edge and is therefore assigned to HF 2. With increasing O content, circumferential crack networks dominate indicating cohesive failure of the thin films [35]. Due to the expanding crack network from 22.2 at.-% O, the AlCrON thin films are ranked HF 3.

The critical loads L_{c2} and L_{c3} that result from the scratch test describe the adhesive failures of the thin film systems and are exemplary shown in Fig. 7. At L_{c2} adhesive failure by chipping of the thin film at the edge of the scratch track appears. Total failure of the thin film by complete exposure of the substrate occurs at L_{c3}.

Apart from the thin film system with O content 38.9 at.-%, all systems exhibit L_{c3} values of >60 N (see Fig. 8) and correspond to the recommended lower limit for industrial applications [55]. For the critical load L_{c2} a decrease with increasing O concentration from (46.32 ± 2.64) N for AlCrN to (15.06 ± 1.66) N for AlCrON deposited at $q_{O2} = 30$ sccm is observed (see Fig. 8). The critical loads L_{c3} show a relatively constant trend with values between 66.23 and 67.44 N except for the drop between 12.2 and 55.3 at.-% O to (58.96 ± 1.27) N. When comparing the values of both critical loads, the drop is also evident for L_{c2}. Additionally, it is noticeable that the hardness H and H/E ratios follow opposite directions. Due to the change to an oxynitridic structure, higher residual stress can be expected because of the lattice distortion and a more brittle character which is evident in the L_{c2} reduction [56,57].

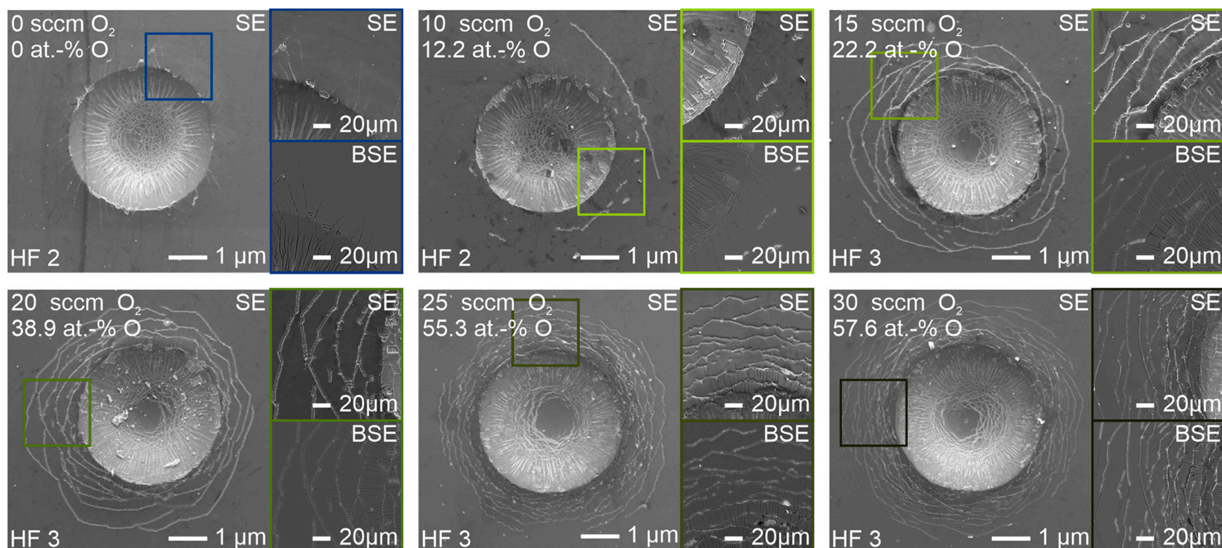

Fig. 6. SEM micrographs of the Rockwell indents of the AlCrN and AlCrON thin film system deposited at different O_2 flow rates q_{O2}/with different O contents.

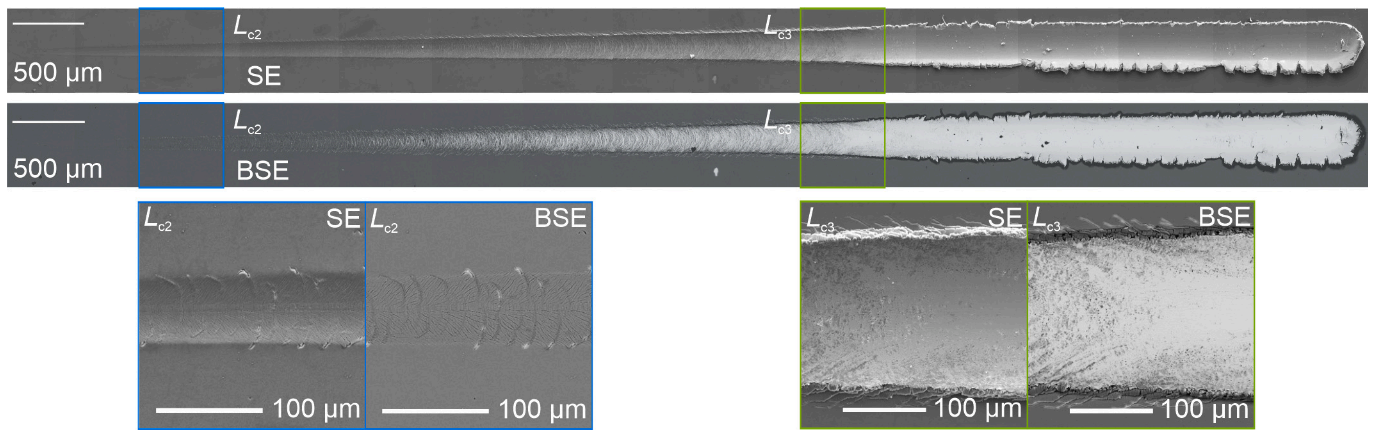

Fig. 7. SEM micrographs of L_{c2} and L_{c3} of an exemplary scratch of AlCrON with thin film deposited at an O_2 gas flow rate q_{O2} = 30 sccm.

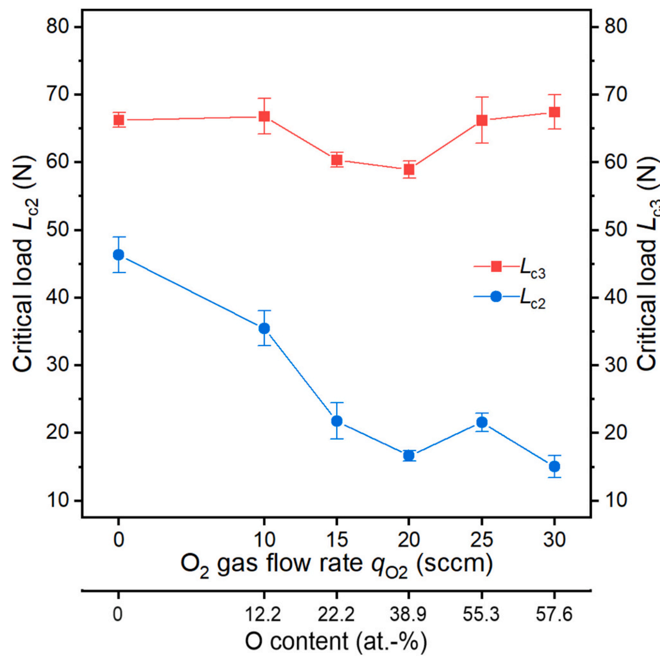

Fig. 8. Critical loads L_{c2} and L_{c3} of the AlCrN and AlCrON thin film system deposited at different O_2 flow rates q_{O2}/with different O contents.

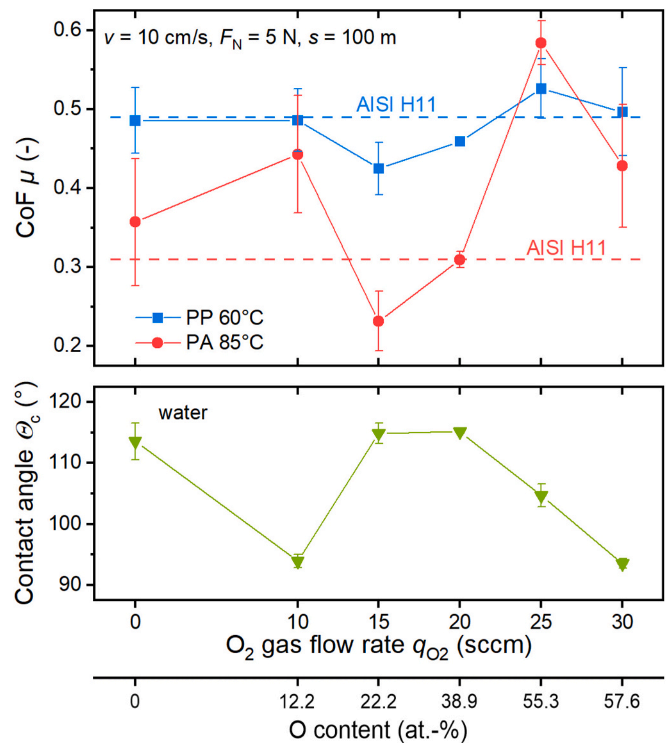

Fig. 9. Coefficient of friction (CoF) μ and wettability of the AlCrN and AlCrON thin films deposited at different O_2 gas flow rates q_{O2}/with different O contents.

3.4. Tribological properties of AlCrON thin films

The tribological tests were carried out against two different common types of plastic PP and PA at operation temperatures of 60 °C and 80 °C, respectively. As the plastics can still melt, due to additional friction heat, the wettability of the thin film surfaces was also taken into account. No abrasive wear could be detected on the AlCrON thin films. Fig. 9 shows that the CoF μ against both plastics exhibit similar behavior. For PP against the uncoated AISI H11, $\mu = 0.49 \pm 0.04$ was measured, and for PA $\mu = 0.31 \pm 0.01$. Against PP AlCrON with 22.2 at.-% and 38.9 at.-% show an lowered CoF with $\mu = 0.43 \pm 0.03$ and $\mu = 0.46 \pm 0.01$. AlCrON deposited at q_{O2} = 25 sccm/55.3 at.-% O exhibits an increased CoF of $\mu = 0.53 \pm 0.04$ while the other thin film systems have similar CoF values like the uncoated steel of 0.49 to 0.50. Against PA only AlCrON with 22.2 at.-% O reaches a decreased friction of $\mu = 0.23 \pm 0.04$. AlCrON with 38.9 at.-% O is close to AISI H11 with $\mu = 0.31 \pm 0.01$. The other thin films range from 0.36 to 0.58 above CoF of the uncoated steel.

Comparing the values of the contact angle Θ_c to the CoF μ shows a reverse trend. The AlCrON thin films with low friction, deposited at an O_2 gas flow rate q_{O2} of 15 sccm and 20 sccm, also show the lowest wettability with a high contact angle of $\Theta_c = (114.9 \pm 1.7)^\circ$ and $\Theta_c = (115.1 \pm 0.3)^\circ$. A lower wettability against water indicates a lower adherence to the coated surface and therefore a reduced CoF μ against molten plastics is expected. The study of Kruppe et al. where AlCrON showed a lower wetting ability compared to AlCrN explained that the contact angle is dependent on the chemical composition [31]. In Ti-doped ZrON thin films higher proportions of TiO_2 increased the wettability [58]. The fact that the friction-reducing effect is more pronounced against PP than against PA can be explained by the polarity of the plastics. PP is non-polar while PA is polar like water and exhibits therefore a lower adherence and lower CoF than PP.

3.5. Electrical properties of AlCrON thin films

As a protective coating, AlCrON requires insulation to ensure the

functionality of the sensor thin films and prevent short circuits. Therefore, the dielectric strength and the electrical resistance were determined. The dielectric strength for the as-deposited AlCrON thin films shows a steep increase from 3 V for AlCrN to 32 V by adding 12.2 at.-% O (see Fig. 10a)). With a further rise in the O concentration, the dielectric strength decreases to 28 V. The reduction of the dielectric strength is related to the decrease of the layer thickness due to a reduced deposition rate with higher O_2 gas flow rates. Normalized to the thin film thicknesses, the dielectric strength shows an increase with higher O content (see Fig. 10a)).

The electrical resistance was measured with applied DC voltages from 2 V to 20 V (see Fig. 10b)). With higher O contents in the AlCrON thin film systems, an increased ionic bonding character is responsible for the rise of the electrical resistivity in the transition regime between the nitridic and oxidic thin films [59]. For the applied voltages, AlCrON behaves similarly with increasing O contents. The AlCrN reference has conductive characteristics and could therefore not be measured. The addition of O increases the electrical resistivity from 92,200 to 1.2×10^9 Ω for 2 V and from 48,200 to 6.2×10^9 Ω for 20 V. Between the O concentration of 38.9 at.-% and 55.3 at.-%, where the oxide transition takes place, the values steeply rise. Higher O contents change the bonding structure within the AlCrON thin films to an ionic bonding type that favors a higher electrical resistivity [59,60]. A decreasing electrical conductivity here results from a higher ratio of ion bondings with increasing oxide concentration. Overall, a higher O content increases the insulation properties of the AlCrON thin films. The dielectric strength can additionally be adjusted by the thin film thickness. The resistance characteristic curves were also determined as a function of increasing voltage (see Fig. 11). The oxynitridic AlCrON thin films exhibit a non-ohmic behavior as the resistance curves are not linear. This means that the resistance decreases with increasing voltage. Whereas the oxidic AlCrON thin films tend to be linear and therefore the resistance behaves ohmic. The non-ohmic characteristic of the oxynitridic AlCrON thin films deposited at 10, 15, and 20 sccm O_2 could result from a higher vacancy density as discussed above. A non-ohmic behavior was also observed for amorphous SiON films where the defect density due to O vacancies affected the electrical properties [61].

4. Conclusion and outlook

The increase of the O_2 gas flow rate q_{O2} in the magnetron sputtering process increases the O content in AlCrON thin films and affects its properties. A change from nitridic to oxynitridic and with an O concentration of 55.3 at.-% to a pure oxide structure is observed. The mechanical properties correlate with the change in the phase composition. The AlCrON thin film with 22.2 at.-% O contains hard AlCrN and Cr_2N phases and favors high hardness and *H/E* ratios. The transformation to a more oxide structure reduces the adhesion strength due to a more brittle character. By changing the chemical composition, the wettability of the surfaces changes and shows a correlation with the CoF against PP and PA. A higher hydrophobic behavior corresponds to a lower CoF due to a decreased attachment of plastic on the AlCrON thin films. The lowest CoF and lowest wettability was found for AlCrON with 22.2 at.-% O. Also the type of plastic, as here PP is non-polar and PA is polar, seems to influence the CoF. The dielectric strength and electrical resistivity increase with a higher O concentration that favors an ionic structure resulting in an insulating behavior. To summarize, adjusting the O content is crucial for tailoring the properties of AlCrON thin films to effectively serve as a protective top layer on sensor thin films in processing different types of plastic. Overviewing the obtained results, the AlCrON thin film deposited at an O_2 gas flow rate of $q_{O2} = 15$ sccm with a 22.2 at.-% O concentration shows promising tribo-mechanical properties as a protective top layer for sensor thin films in plastic processing of PP and PA. Subsequently, the AlCrON thin films will be applied as a protective top layer on sensor thin films and the performance of both the AlCrON and the functional thin films will be tested on Hot Ends in fused layer modeling processes with different types of plastic.

CRediT authorship contribution statement

Wolfgang Tillmann: Writing – review & editing, Supervision, Resources. **Julia Urbanczyk:** Writing – original draft, Visualization, Investigation, Conceptualization. **Maximilian Sonnhof:** Investigation. **Bernd Künne:** Writing – review & editing. **Michael Mainz:** Writing – review & editing, Investigation. **Philipp Bengfort:** Writing – review & editing, Investigation. **Hans-Georg Rademacher:** Writing – review & editing, Investigation. **Nelson Filipe Lopes Dias:** Writing – review & editing, Supervision.

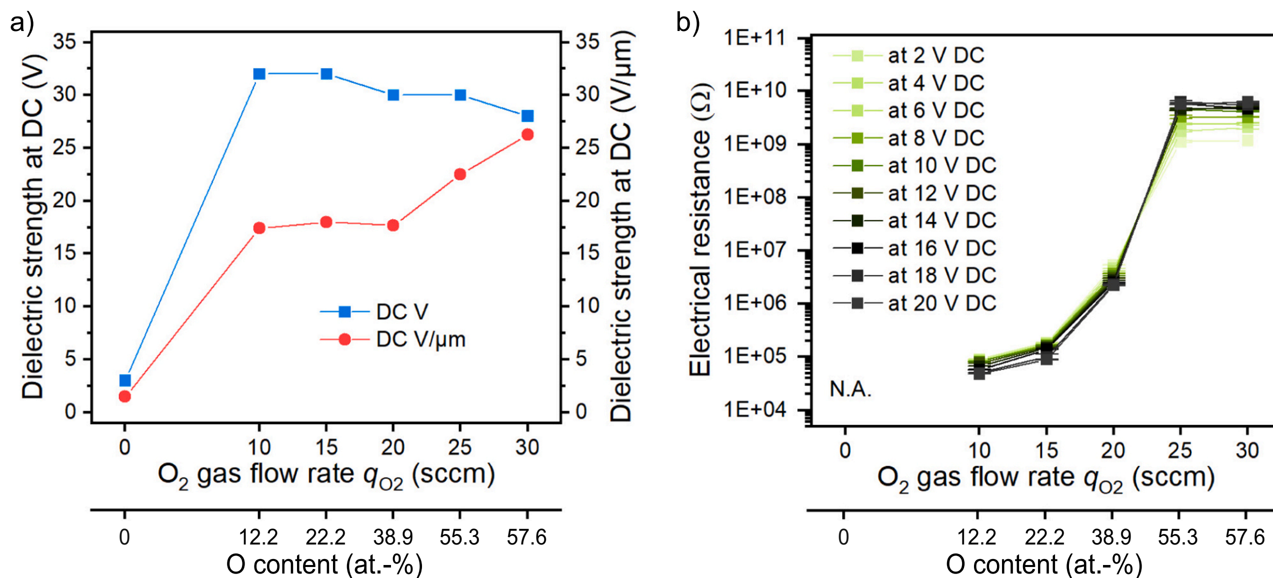

Fig. 10. a) Dielectric strength and b) electrical resistance measured at DC voltages of the AlCrN and AlCrON thin films deposited at different O_2 gas flow rates q_{O2}/ different O contents.

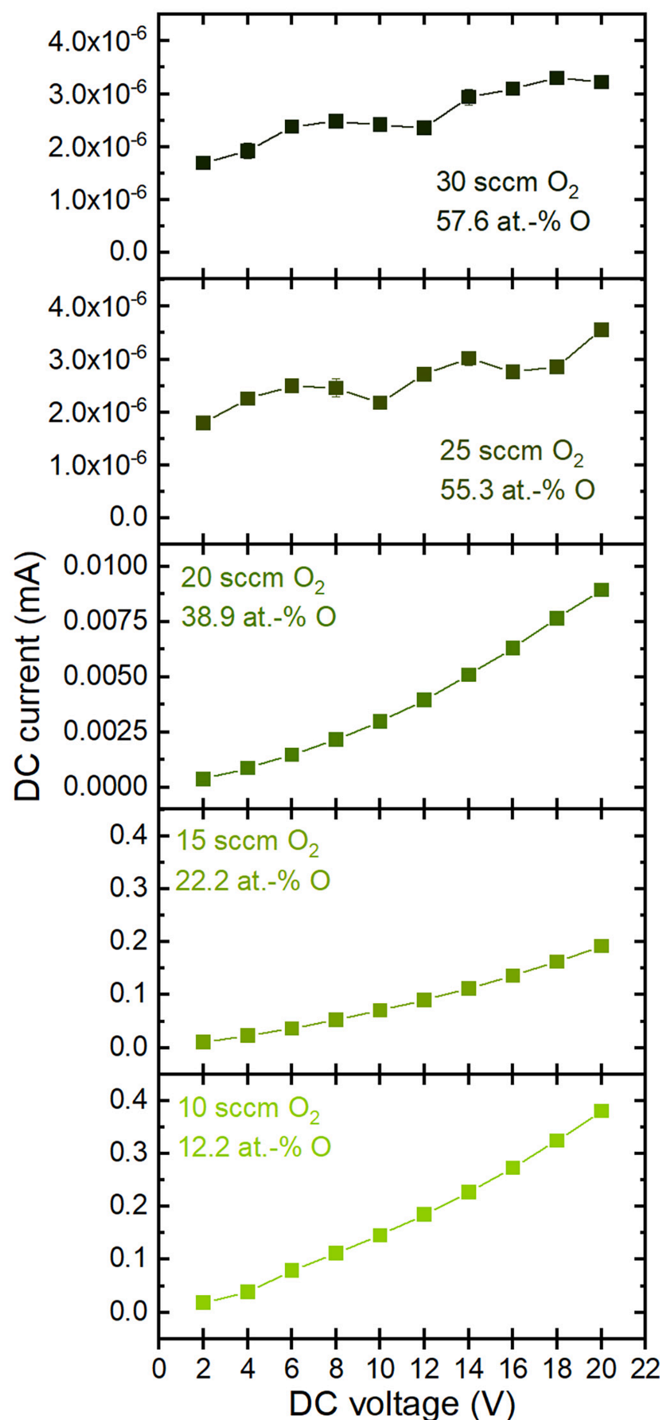

Fig. 11. Resistance characteristic as a function of DC voltage of the AlCrON thin films deposited at different O_2 gas flow rates q_{O2}/different O contents.

Declaration of Generative AI and AI-assisted technologies in the writing process

During the preparation of this work, the authors used ChatGPT (https://chat.openai.com/) to improve the readability of the paper. After using this tool, the authors reviewed and edited the content as needed and take full responsibility for the content of the publication.

Declaration of competing interest

The authors declare that they have no known competing financial interests or personal relationships that could have appeared to influence the work reported in this paper.

Acknowledgments

The authors gratefully acknowledge the financial support of the German Federation of Industrial Research Associations (AiF) for the project 22632 N and the Plastics Research Society registered association (FGK).

Data availability

Data will be made available on request.

References

[1] E. Cuan-Urquizo, E. Barocio, V. Tejada-Ortigoza, R.B. Pipes, C.A. Rodriguez, A. Roman-Flores, Characterization of the mechanical properties of FFF structures and materials: a review on the experimental, computational and theoretical approaches, Materials (Basel, Switzerland) 12 (2019), https://doi.org/10.3390/ma12060895.
[2] A. Jaisingh Sheoran, H. Kumar, Fused deposition modeling process parameters optimization and effect on mechanical properties and part quality, review and reflection on present research, Materials Today: Proceedings 21 (2020) 1659–1672, https://doi.org/10.1016/j.matpr.2019.11.296.
[3] S.A. Tronvoll, S. Popp, C.W. Elverum, T. Welo, Investigating pressure advance algorithms for filament-based melt extrusion additive manufacturing: theory, practice and simulations, RPJ 25 (2019) 830–839, https://doi.org/10.1108/RPJ-10-2018-0275.
[4] M.M. Mbow, P.R. Marin, F. Pourroy, Extruded diameter dependence on temperature and velocity in the fused deposition modeling process, Prog Addit Manuf 5 (2020) 139–152, https://doi.org/10.1007/s40964-019-00107-4.
[5] Wohlers Associates, Wohlers Report: Additive Manufacturing and 3D Printing State of the Industry; Annual Worldwide Progress Report, 2020.
[6] M. Plogmeyer, G. González, C. Pongratz, A. Schott, V. Schulze, G. Bräuer, Tool-integrated thin-film sensor systems for measurement of cutting forces and temperatures during machining, Prod. Eng. Res. Devel. doi:https://doi.org/10.1007/s11740-023-01251-1.
[7] W. Tillmann, D. Kokalj, D. Stangier, V. Schöppner, H.B. Benis, H. Malatyali, Influence of Cr-content on the thermoelectric and mechanical properties of NiCr thin film thermocouples synthesized on thermally sprayed Al2O3, Thin Solid Films 663 (2018) 148–158, https://doi.org/10.1016/j.tsf.2018.08.023.
[8] W. Tillmann, D. Kokalj, D. Stangier, V. Schöppner, H. Malatyali, Combining thermal spraying and magnetron sputtering for the development of Ni/Ni-20Cr thin film thermocouples for plastic flat film extrusion processes, Coatings 9 (2019) 603, https://doi.org/10.3390/coatings9100603.
[9] A. Kantaros, E. Soulis, F.I.T. Petrescu, T. Ganetsos, Advanced composite materials utilized in FDM/FFF 3D printing manufacturing processes: the case of filled filaments, Materials (Basel, Switzerland) 16 (2023), https://doi.org/10.3390/ma16186210.
[10] X. Gao, D. Zhang, S. Qi, X. Wen, Y. Su, Mechanical properties of 3D parts fabricated by fused deposition modeling: effect of various fillers in polylactide, J. Appl. Polym. Sci. 136 (2019), https://doi.org/10.1002/app.47824.
[11] H. Mei, Z. Ali, I. Ali, L. Cheng, Tailoring strength and modulus by 3D printing different continuous fibers and filled structures into composites, Adv. Compos. Hybrid Mater. 2 (2019) 312–319, https://doi.org/10.1007/s42114-019-00087-7.
[12] A. Baptista, F. Silva, J. Porteiro, J. Míguez, G. Pinto, Sputtering physical vapour deposition (PVD) coatings: a critical review on process improvement and market trend demands, Coatings 8 (2018) 402, https://doi.org/10.3390/coatings8110402.
[13] C. Christensen, R. de Reus, S. Bouwstra, Tantalum oxide thin films as protective coatings for sensors, J. Micromech. Microeng. 9 (1999) 113–118, https://doi.org/10.1088/0960-1317/9/2/003.
[14] X. Jin, B. Ma, J. Deng, J. Luo, W. Yuan, High temperature failure modes of In2O3 thin films and improved thermal stability using Al2O3/ZrO2 protective layers, Ceram. Int. 47 (2021) 28411–28418, https://doi.org/10.1016/j.ceramint.2021.06.258.
[15] M. Heinze, Wear resistance of hard coatings in plastics processing, Surf. Coat. Technol. 105 (1998) 38–44, https://doi.org/10.1016/S0257-8972(98)00449-6.
[16] L. Cunha, M. Andritschky, K. Pischow, Z. Wang, A. Zarychta, A.S. Miranda, A. M. Cunha, Performance of chromium nitride based coatings under plastic processing conditions, Surf. Coat. Technol. 133-134 (2000) 61–67, https://doi.org/10.1016/S0257-8972(00)00875-6.
[17] L. Cunha, M. Andritschky, Residual stress, surface defects and corrosion resistance of CrN hard coatings, Surf. Coat. Technol. 111 (1999) 158–162, https://doi.org/10.1016/S0257-8972(98)00731-2.
[18] Y.C. Chim, X.Z. Ding, X.T. Zeng, S. Zhang, Oxidation resistance of TiN, CrN, TiAlN and CrAlN coatings deposited by lateral rotating cathode arc, Thin Solid Films 517 (2009) 4845–4849, https://doi.org/10.1016/j.tsf.2009.03.038.
[19] M. Uchida, N. Nihira, A. Mitsuo, K. Toyoda, K. Kubota, T. Aizawa, Friction and wear properties of CrAlN and CrVN films deposited by cathodic arc ion plating

method, Surf. Coat. Technol. 177-178 (2004) 627–630, https://doi.org/10.1016/S0257-8972(03)00937-X.
[20] J. Lin, B. Mishra, J.J. Moore, W.D. Sproul, A study of the oxidation behavior of CrN and CrAlN thin films in air using DSC and TGA analyses, Surf. Coat. Technol. 202 (2008) 3272–3283, https://doi.org/10.1016/j.surfcoat.2007.11.037.
[21] G. Biava, I.B. de Araujo Fernandes Siqueira, R.F. Vaz, G.B. de Souza, H.C.M. Jambo, A. Szogyenyi, A.G. Pukasiewicz, Evaluation of high temperature corrosion resistance of CrN, AlCrN, and TiAlN arc evaporation PVD coatings deposited on Waspaloy, Surf. Coat. Technol. 438 (2022) 128398. doi:https://doi.org/10.1016/j.surfcoat.2022.128398.
[22] R. K., P. S., Corrosion of metal – oxide systems, in: H. Shih (Ed.), Corrosion Resistance, InTech, 2012.
[23] R. Cremer, M. Witthaut, K. Reichert, D. Neuschütz, Surface and interface analysis of PVD Al-O-N and γ-Al 2 O 3 diffusion barriers, Fresenius J. Anal. Chem. 365 (1999) 158–162, https://doi.org/10.1007/s002160051464.
[24] Q.M. Wang, Y.N. Wu, M.H. Guo, P.L. Ke, J. Gong, C. Sun, L.S. Wen, Ion-plated Al–O–N and Cr–O–N films on Ni-base superalloys as diffusion barriers, Surf. Coat. Technol. 197 (2005) 68–76, https://doi.org/10.1016/j.surfcoat.2004.09.022.
[25] R. Raab, C.M. Koller, S. Kolozsvári, J. Ramm, P.H. Mayrhofer, Thermal stability of arc evaporated Al-Cr-O-N coatings, Surf. Coat. Technol. 356 (2018) 64–71, https://doi.org/10.1016/j.surfcoat.2018.09.036.
[26] E. Almandoz, J. Fernández de Ara, J. Martínez de Bujanda, J. Fernández Palacio, R. J. Rodríguez, Z. Zhang, H. Dong, Y. Qin, G. García Fuentes, CrAlON CAE-PVD coatings for oxidation and wear protection of TZM alloys in FAST sintering applications, Mater. Chem. Phys. 208 (2018) 189–197, https://doi.org/10.1016/j.matchemphys.2018.01.056.
[27] F. Ahmad, L. Zhang, J. Zheng, I. Sidra, F. Cai, S. Zhang, Structural evolution and high-temperature tribological properties of AlCrON coatings deposited by multi-arc ion plating, Ceram. Int. 46 (2020) 24281–24289, https://doi.org/10.1016/j.ceramint.2020.06.208.
[28] H. Najafi, A. Karimi, P. Dessarzin, M. Morstein, Correlation between anionic substitution and structural properties in AlCr(OxN1−x) coatings deposited by lateral rotating cathode arc PVD, Thin Solid Films 520 (2011) 1597–1602, https://doi.org/10.1016/j.tsf.2011.08.075.
[29] K. Bobzin, R. Nickel, N. Bagcivan, F.D. Manz, PVD—coatings in injection molding machines for processing optical polymers, Plasma Process. Polym. 4 (2007) S144–S149, https://doi.org/10.1002/ppap.200730507.
[30] K. Bobzin, T. Brögelmann, C. Kalscheuer, M. Naderi, Hybrid dcMS/HPPMS PVD nitride and oxynitride hard coatings for adhesion and abrasion reduction in plastics processing, Surf. Coat. Technol. 308 (2016) 349–359, https://doi.org/10.1016/j.surfcoat.2016.07.103.
[31] K. Bobzin, T. Brögelmann, G. Grundmeier, T. de los Arcos, M. Wiesing, N. C. Kruppe, et al., Surf. Coat. Technol. 308 (2016) 394–403, https://doi.org/10.1016/j.surfcoat.2016.07.093.
[32] N. Bagcivan, K. Bobzin, T. Brögelmann, C. Kalscheuer, Development of (Cr,Al)ON coatings using middle frequency magnetron sputtering and investigations on tribological behavior against polymers, Surf. Coat. Technol. 260 (2014) 347–361. doi:https://doi.org/10.1016/j.surfcoat.2014.09.016.
[33] W.C. Oliver, G.M. Pharr, An improved technique for determining hardness and elastic modulus using load and displacement sensing indentation experiments, J. Mater. Res. 7 (1992) 1564–1583, https://doi.org/10.1557/JMR.1992.1564.
[34] Y.-Y. Chang, S.-Y. Weng, C.-H. Chen, F.-X. Fu, High temperature oxidation and cutting performance of AlCrN, TiVN and multilayered AlCrN/TiVN hard coatings, Surf. Coat. Technol. 332 (2017) 494–503, https://doi.org/10.1016/j.surfcoat.2017.06.080.
[35] DIN 4856:2018-02, Kohlenstoffschichten und andere Hartstoffschichten_-Rockwell-Eindringprüfung zur Bewertung der Haftung, Beuth Verlag GmbH, Berlin.
[36] DIN EN ISO 20502:2016-11, Hochleistungskeramik_-Bestimmung der Haftung von keramischen Schichten mit dem Ritztest (ISO_20502:2005 einschließlich Cor_1: 2009); Deutsche Fassung EN_ISO_20502:2016, Beuth Verlag GmbH, Berlin.
[37] G. Erhard, Konstruieren mit Kunststoffen, 4th ed., Hanser, München, 2008.
[38] O. Schwarz, F.W. Ebeling, H. Huberth, F. Richter, H. Schirber, N. Schlör, Kunststoffkunde: Aufbau, Eigenschaften, Verarbeitung, Anwendungen der Thermoplaste, Duroplaste und Elastomere, 10th ed., Vogel Business Media, Würzburg, 1987.
[39] W. Tillmann, N.F. Lopes Dias, D. Stangier, N. Gelinski, Tribological performance of PVD film systems against plastic counterparts for adhesion-reducing application in injection molds, Coatings 9 (2019) 588, https://doi.org/10.3390/coatings9090588.
[40] D.Y. Kwok, A.W. Neumann, Contact angle measurement and contact angle interpretation, Adv. Colloid Interf. Sci. 81 (1999) 167–249, https://doi.org/10.1016/S0001-8686(98)00087-6.
[41] Z.R. Liu, J.W. Du, L. Chen, Influence of oxygen content on structure, thermal stability, oxidation resistance, and corrosion resistance of arc evaporated (Cr, Al)N coatings, Surf. Coat. Technol. 432 (2022) 128057, https://doi.org/10.1016/j.surfcoat.2021.128057.
[42] Thomas C. Allison, NIST-JANAF Thermochemical Tables - SRD 13, National Institute of Standards and Technology, 2013.
[43] A. Khatibi, J. Sjölen, G. Greczynski, J. Jensen, P. Eklund, L. Hultman, Structural and mechanical properties of Cr–Al–O–N thin films grown by cathodic arc deposition, Acta Mater. 60 (2012) 6494–6507, https://doi.org/10.1016/j.actamat.2012.08.010.
[44] H. Willmann, P.H. Mayrhofer, P. Persson, A.E. Reiter, L. Hultman, C. Mitterer, Thermal stability of Al–Cr–N hard coatings, Scr. Mater. 54 (2006) 1847–1851, https://doi.org/10.1016/j.scriptamat.2006.02.023.
[45] W.M. Haynes (Ed.), CRC Handbook of Chemistry and Physics, 97th ed., CRC Press, Boca Raton, London, New York, 2017.
[46] W. Siriprom, C. Chananonnawathorn, S. Kongsriprapan, K. Teanchai, Herman, M. Horprathum, Preparation and characterization of CrN thin film by DC reactive magnetron sputtering, Materials Today: Proceedings 5 (2018) 15224–15227, https://doi.org/10.1016/j.matpr.2018.04.087.
[47] B. Wei, H. Liang, D. Zhang, Z. Wu, Z. Qi, Z. Wang, CrN thin films prepared by reactive DC magnetron sputtering for symmetric supercapacitors, J. Mater. Chem. A 5 (2017) 2844–2851, https://doi.org/10.1039/C6TA09985H.
[48] J. Schulte, G. Sobe, Magnetron sputtering of aluminium using oxygen or nitrogen as reactive gas, Thin Solid Films 324 (1998) 19–24, https://doi.org/10.1016/S0040-6090(97)01197-8.
[49] E. Almandoz, G.G. Fuentes, J. Fernández, J.M. de Bujanda, R.J. Rodríguez, F. J. Pérez-Trujillo, G. Alcalá, A. Lousa, Y. Qin, Chemical and mechanical stability of air annealed cathodic arc evaporated CrAlON coatings, Surf. Coat. Technol. 351 (2018) 153–161, https://doi.org/10.1016/j.surfcoat.2018.07.081.
[50] Y. Gao, F. Cai, W. Fang, Y. Chen, S. Zhang, Q. Wang, Effect of oxygen content on wear and cutting performance of AlCrON coatings, J. Mater. Eng. Perform. 28 (2019) 828–837, https://doi.org/10.1007/s11665-018-3823-7.
[51] A. Karimi, M. Morstein, T. Cselle, Influence of oxygen content on structure and properties of multi-element AlCrSiON oxynitride thin films, Surf. Coat. Technol. 204 (2010) 2716–2722, https://doi.org/10.1016/j.surfcoat.2010.02.029.
[52] F. Ahmad, L. Zhang, J. Zheng, I. Sidra, S. Zhang, Characterization of AlCrN and AlCrON coatings deposited on plasma nitrided AISI H13 steels using ion-source-enhanced arc ion plating, Coatings 10 (2020) 306, https://doi.org/10.3390/coatings10040306.
[53] H. Najafi, A. Karimi, M. Morstein, Microstructure of Al95.5Cr2.5Si2(N1−xOx) thin films covering from nitrides to oxides, Surf. Coat. Technol. 205 (2011) 5199–5204, https://doi.org/10.1016/j.surfcoat.2011.05.031.
[54] J. Musil, Hard and superhard nanocomposite coatings, Surf. Coat. Technol. 125 (2000) 322–330, https://doi.org/10.1016/S0257-8972(99)00586-1.
[55] S. Ma, J. Procházka, P. Karvánková, Q. Ma, X. Niu, X. Wang, D. Ma, K. Xu, S. Veprek, Comparative study of the tribological behaviour of superhard nanocomposite coatings nc-TiN/a-Si3N4 with TiN, Surf. Coat. Technol. 194 (2005) 143–148, https://doi.org/10.1016/j.surfcoat.2004.05.007.
[56] A. Munteanu, D. Munteanu, B. Borcea, F. Vaz, L. Cunha, C. Olteanu, The influence of the deposition conditions on the mechanical properties of TI(C,O,N) thin films obtained by sputtering process, Metalurgia Int. 14 (2009) 129–132.
[57] O. Banakh, C. Csefalvay, P.-A. Steinmann, M. Fenker, H. Kappl, Evaluation of adhesion and tribological behaviour of tantalum oxynitride thin films deposited by reactive magnetron sputtering onto steel substrates, Surf. Coat. Technol. 200 (2006) 6500–6504, https://doi.org/10.1016/j.surfcoat.2005.11.079.
[58] D. Cristea, A.I. Scărlătescu, C. Croitoru, A. Marin, I.-L. Velicu, V. Tiron, D. Martínez-Martínez, C.S. Da Oliveira, L. Cunha, Photocatalytical and corrosion behavior of sputtered zirconium oxynitride thin films doped with titanium, Surfaces and Interfaces 42 (2023) 103488, https://doi.org/10.1016/j.surfin.2023.103488.
[59] P. Carvalho, J.M. Chappé, L. Cunha, S. Lanceros-Méndez, P. Alpuim, F. Vaz, E. Alves, C. Rousselot, J.P. Espinós, A.R. González-Elipe, Influence of the chemical and electronic structure on the electrical behavior of zirconium oxynitride films, J. Appl. Phys. 103 (2008), https://doi.org/10.1063/1.2927494.
[60] J.-M. Chappé, N. Martin, J.F. Pierson, G. Terwagne, J. Lintymer, J. Gavoille, J. Takadoum, Influence of substrate temperature on titanium oxynitride thin films prepared by reactive sputtering, Appl. Surf. Sci. 225 (2004) 29–38, https://doi.org/10.1016/j.apsusc.2003.09.028.
[61] H.M.A. El-Oyoun, T. Inokuma, Y. Kurata, S. Hasegawa, Structural properties of ultrathin amorphous silicon oxynitride layers, Jpn. J. Appl. Phys. 42 (2003) 3570–3577, https://doi.org/10.1143/JJAP.42.3570.